# Strength Evaluation of Electronic Plastic Packages Using Stress Intensity Factors of V-Notch

**Toru Ikeda**[1], **Isao Arase, Yuya Ueno, Noriyuki Miyazaki**

**Abstract:** In electronic devices, the corners of joined dissimilar materials exist between plastic resin and a die pad or a chip. Failure of the plastic resin is often caused from these corners during the assembly process or the operation of products. The strength evaluation of the corner is important to protect the failure of plastic packages. To evaluate the singular stress field around a corner, we utilize the stress intensity factors of the asymptotic solution for a corner of joined dissimilar materials. We show that the accurate stress intensity factor can be analyzed by the displacement extrapolation method using the displacement obtained from the finite element method, and the resulting stress intensity factor can be utilized for the evaluation of the strength of the corner in electronic devices.

**keyword:** fracture mechanics, stress intensity factor, corner, electronic packaging

## 1 Introduction

A plastic package is a common electronic packaging technique at the present time. The strength of a plastic package is very important for the reliability of an electronic product. Crack occurrence in molding resin during the solder reflow process, temperature accelerated tests or the operation of products is a main cause of the failure of a plastic package.

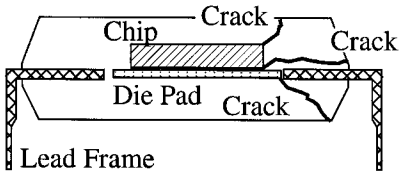


**Figure 1** : Failures in an electronic device.

Nishimura, Hirose, and Tanaka (1993); Tanaka and Nishiura (1994); Ikeda, Komohara, and Miyazaki (1997) applied fracture mechanics to the evaluation of the delamination of an interface crack between molding resin and a lead frame in a plastic package. They have presented the delamination criterion of the interface crack between molding resin and a leadframe. The extension of the interface crack, which is assumed to have a small length, is predicted using this criterion. These methods are useful for the design of plastic packages. However, a preassumed delamination length is ambiguous. We cannot also estimate the crack initiation in molding resin by these methods. These cracks are often initiated at the corners in molding resin as shown in Fig. 1. The strength of the corners should be evaluated for the reliability of electronic devices; however, it is difficult because of the stress singularity around a corner which is similar to that around a crack tip. The simple evaluation technique for the strength of corners in electronic devices is desired.

Nishimura, Tatemichi, Miura, and Sakamoto (1987); Nishimura, Kawai, and Murakami (1989) evaluated the fatigue crack propagation from a corner of a die pad in an IC plastic package using a stress value near a corner obtained by the finite element method (FEM). Kitano, Kawai, Nishimura, and Nishi (1989) estimated the crack initiation from a corner in molding resin during the solder reflow process by a similar method. These methods are practical, but a stress value near a corner directly obtained by the FEM depends on the mesh size around the corner. Hattori, Nishimura, and Murakami (1990) utilized a stress singularity parameter at a corner for the strength evaluation of an IC chip instead of a stress value near the corner. They obtained the order of stress singularity using the eigenfunction expansion method, which was originally presented by Williams (1952), and estimated its stress intensity factor by extrapolating the stress data obtained by the FEM. Dunn and Suwito (1997); Dunn, Suwito, Cunningham, and May (1997) measured the mixed mode fracture toughness of a v-notch using the stress intensity factors of a v-notch, which was also obtained by the William's eigenfunction expansion method and the FEM.

In this study, we utilize the explicit asymptotic solution around a corner of joined dissimilar materials and its stress intensity factors proposed by Chen and Nishitani (1991) instead of the William's eigenfunction expansion method and its asymptotic function. We developed the stress and displacement extrapolation methods for calculating the stress intensity factors of a corner of joined dissimilar materials. This technique can produce accurate stress intensity factors at a corner using a relative coarse finite element mesh.

The stress intensity factor of a v-notched three point bending specimen of the molding resin for an actual plastic package

[1] Chemical Engineering Group, Department of Materials Process Engineering, Kyushu University, 6-10-1, Hakozaki, Higashi-ku, Fukuoka, 812-8581, Japan. E-mail: ikeda@chem-eng.kyushu-u.ac.jp

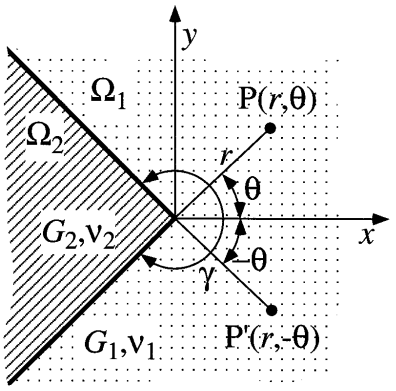


**Figure 2** : Coordinate system around a corner of jointed dissimilar materials.

was analyzed. Fracture tests of the three point bending specimens were performed, and the critical stress intensity factor of a corner at fracture (the fracture toughness of a corner) for the molding resin was measured.

## 2 Asymptotic solution in the vicinity of a corner of joined dissimilar materials

Chen and Nishitani (1991) derived the asymptotic solution in the vicinity of a corner of joined dissimilar materials as shown in Fig. 2. The orders of stress singularity for the symmetric deformation (mode I) and the skew-symmetric deformation (mode II) to the $x$-axis, $1-\lambda_1$ and $1-\lambda_2$, are obtained from the following characteristic equations.

$$\begin{aligned} D_1(\alpha,\beta,\gamma,\lambda) &= (\alpha-\beta)^2\lambda^2(1-\cos 2\gamma) \\ &+ 2\lambda(\alpha-\beta)\sin\gamma\{\sin\lambda\gamma+\sin\lambda(2\pi-\gamma)\} \\ &+ 2\lambda(\alpha-\beta)\beta\sin\gamma\{\sin\lambda(2\pi-\gamma)-\sin\lambda\gamma\} \\ &+ (1-\alpha^2)-(1-\beta^2)\cos 2\lambda\pi \\ &+ (\alpha^2-\beta^2)\cos\{2\lambda(\gamma-\pi)\} = 0 \end{aligned} \tag{1}$$

$$\begin{aligned} D_2(\alpha,\beta,\gamma,\lambda) &= (\alpha-\beta)^2\lambda^2(1-\cos 2\gamma) \\ &- 2\lambda(\alpha-\beta)\sin\gamma\{\sin\lambda\gamma+\sin\lambda(2\pi-\gamma)\} \\ &- 2\lambda(\alpha-\beta)\beta\sin\gamma\{\sin\lambda(2\pi-\gamma)-\sin\lambda\gamma\} \\ &+ (1-\alpha^2)-(1-\beta^2)\cos 2\lambda\pi \\ &+ (\alpha^2-\beta^2)\cos\{2\lambda(\gamma-\pi)\} = 0 \end{aligned} \tag{2}$$

where $\alpha$ and $\beta$ are Dunders parameters as

$$\begin{aligned} \alpha &= \frac{G_1(\kappa_2+1)-G_2(\kappa_1+1)}{G_1(\kappa_2+1)+G_2(\kappa_1+1)}, \\ \beta &= \frac{G_1(\kappa_2-1)-G_2(\kappa_1-1)}{G_1(\kappa_2+1)+G_2(\kappa_1+1)} \end{aligned} \tag{3}$$

$$\kappa_i = \begin{cases} (3-\nu_i)/(1+\nu_i) & \text{plane stress} \\ 3-4\nu_i & \text{plane strain} \end{cases} \tag{4}$$

where $i$ takes material 1 ($i=1$) or material 2 ($i=2$), ($G_1$, $G_2$) and ($\nu_1$, $\nu_2$) are shear moduli and Poisson's ratios for the material 1 and 2 respectively. A unique real solution $\lambda_2$ can be obtained from Eq. 2 for all combinations of materials. If the combination is selected according to the next equation, a unique real solution $\lambda_1$ also can be obtained from Eq. 1.

$$\beta(\alpha-\beta) > 0 \tag{5}$$

The range expressed by Eq. 5 was found out numerically by Chen and Nishitani (1991). Fortunately, almost all combinations of actual materials are within the range of Eq. 5. The stress field in the vicinity of a corner of joined dissimilar materials selected according to the Eq. 5 is shown as

$$\sigma_{kl,i} = \frac{K_{I,\lambda_1}}{r^{1-\lambda_1}} f^I_{kl,i}(\theta) + \frac{K_{II,\lambda_2}}{r^{1-\lambda_2}} f^{II}_{kl,i}(\theta) \tag{6}$$

where $\sigma_{kl,i}$ ($kl = xx, yy, xy$) is the stress in the region of material $i$, $K_{I,\lambda_1}$ and $K_{II,\lambda_2}$ are the stress intensity factors of a corner for Mode I and Mode II deformations respectively; $f^I_{kl,i}(\theta)$ and $f^{II}_{kl,i}(\theta)$ are the coefficient functions of $\theta$, whose details are shown in Appendix A. The displacements around a corner are also described by the stress intensity factors $K_{I,\lambda_1}$ and $K_{II,\lambda_2}$ as

$$\begin{cases} u_1 = \dfrac{r^{\lambda_1}K_{I,\lambda_1}}{2\sqrt{2\pi}G_1} g^I_{1,1}(\theta) + \dfrac{r^{\lambda_2}K_{II,\lambda_2}}{2\sqrt{2\pi}G_1} g^{II}_{1,1}(\theta) \\ v_1 = \dfrac{r^{\lambda_1}K_{I,\lambda_1}}{2\sqrt{2\pi}G_1} g^I_{2,1}(\theta) + \dfrac{r^{\lambda_2}K_{II,\lambda_2}}{2\sqrt{2\pi}G_1} g^{II}_{2,1}(\theta) \end{cases} \tag{7}$$

where $u_1$ and $v_1$ are components of the displacement for $x$ and $y$ directions in the region of material 1, $g^I_{1,1}(\theta)$, $g^{II}_{1,1}(\theta)$, $g^I_{2,1}(\theta)$ and $g^{II}_{2,1}(\theta)$ are the coefficient functions of $\theta$, whose details are shown in Appendix B.

## 3 Analysis of the stress intensity factor of a corner

### *3.1 Stress extrapolation method*

The coefficient functions $f^{II}_{xx,1}(\theta)$, $f^{II}_{yy,1}(\theta)$ and $f^I_{xy,1}(\theta)$ in Eq. 6 are 0 at $\theta = 0$.

$$f^{II}_{xx,1}(0) = f^{II}_{yy,1}(0) = f^I_{xy,1}(0) = 0 \tag{8}$$

Substituting Eq. 8 into Eq. 6, the following equations for the stress extrapolation method are derived as

$$\begin{cases} K_{I,\lambda_1} = \lim\limits_{r\to 0} \left(\sigma_{xx,1} \big/ f^I_{xx,1}(0)\right) r^{1-\lambda_1} \\ K_{I,\lambda_1} = \lim\limits_{r\to 0} \left(\sigma_{yy,1} \big/ f^I_{yy,1}(0)\right) r^{1-\lambda_1} \\ K_{II,\lambda_2} = \lim\limits_{r\to 0} \left(\sigma_{xy,1} \big/ f^{II}_{xy,1}(0)\right) r^{1-\lambda_2} \end{cases} \tag{9}$$

The stress intensity factors $K_{I,\lambda_1}$ and $K_{II,\lambda_2}$ in Eq. 9 are calculated from the stress on the $x$-axis near the corner obtained by a numerical analysis such as the FEM. The stress intensity factors $K_{I,\lambda_1}$ and $K_{II,\lambda_2}$ at $r=0$ can be extrapolated as Fig. 3.

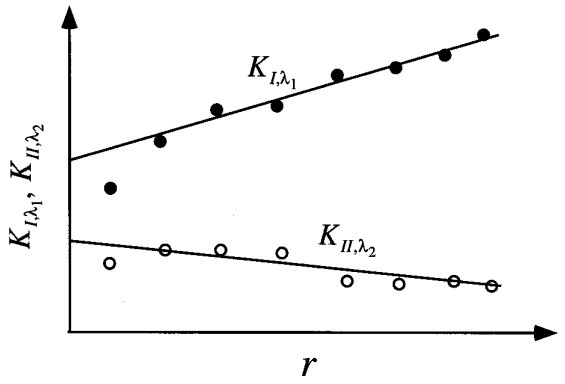


**Figure 3** : Schematic example of the stress extrapolation method.

### *3.2 Displacement extrapolation method*

Displacement can be obtained more accurately than stress using a numerical analysis such as the FEM . So the displacement extrapolation method is superior to the stress extrapolation method for the stress intensity factor analysis. The displacements are separated into the mode I component ($u_1^I$, $v_1^I$) and the mode II component ($u_1^{II}$, $v_1^{II}$) using the respective displacements at the point $P$ and the point $P'$ as shown in Fig. 2 which are symmetric with respect to $x$-axis.

$$\begin{cases} u_1^I = \frac{1}{2}\left(u_1^{(1)} + u_1^{(2)}\right) \\ v_1^I = \frac{1}{2}\left(v_1^{(1)} - v_1^{(2)}\right) \end{cases} \qquad \begin{cases} u_1^{II} = \frac{1}{2}\left(u_1^{(1)} - u_1^{(2)}\right) \\ v_1^{II} = \frac{1}{2}\left(v_1^{(1)} + v_1^{(2)}\right) \end{cases} \tag{10}$$

where ($u_1^{(1)}$, $v_1^{(1)}$) and ($u_1^{(2)}$, $v_1^{(2)}$) are the respective displacements at the point $P$ and the point $P'$ in the material 1. The stress intensity factors $K_{I,\lambda_1}$ and $K_{II,\lambda_2}$ are obtained by the displacement extrapolation method using the following equations, in the same way as the stress extrapolation method.

$$K_{I,\lambda_1} = \lim_{r\to 0} \frac{2\sqrt{2\pi}G_1 v_1^I}{r^{\lambda_1}\left[\left(A_1^I\kappa_1 + B_1^I\right)\sin(\lambda_1\theta) - A_1^I\lambda_1\sin\left((2-\lambda_1)\theta\right)\right]},$$
$$K_{II,\lambda_2} = \lim_{r\to 0} \frac{2\sqrt{2\pi}G_1 u_1^{II}}{r^{\lambda_2}\left[\left(A_1^{II}\kappa_1 - B_1^{II}\right)\sin(\lambda_2\theta) + A_1^{II}\lambda_2\sin\left((2-\lambda_2)\theta\right)\right]} \tag{11}$$

where

$$\begin{cases} A_1^I = \sin\{\lambda_1(\gamma-\pi)\} \\ B_1^I = \dfrac{\lambda_1(\alpha-\beta)\sin\{\gamma-\lambda_1(\gamma-\pi)\} + (1-\beta)\sin(\lambda_1\pi)}{\alpha-\beta} \\ A_1^{II} = \sin\{\lambda_2(\gamma-\pi)\} \\ B_1^{II} = \dfrac{\lambda_2(\alpha-\beta)\sin\{\gamma-\lambda_2(\gamma-\pi)\} - (1-\beta)\sin(\lambda_2\pi)}{\alpha-\beta} \end{cases} \tag{12}$$

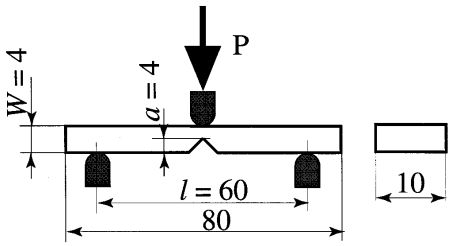


**Figure 4** : V-notched three point bending specimen.

**Table 1** : Obtained values for the stress intensity factor of the corner of a v-notch.

| Mesh Type | Minimum Element (mm) | Number of Nodes | $F_{I,\lambda_1}$ Stress Method | Disp. Method |
|---|---|---|---|---|
| A | 0.0002 | 3353 | 2.78 | 2.99 |
| B | 0.0200 | 1914 | 3.00 | 2.98 |
| C | 0.1300 | 1375 | failure | 3.06 |
| D | 0.2200 | 903 | failure | 3.06 |

Stress Method: Stress extrapolation method
Disp. Method: Displacement extrapolation method

### *3.3 Stress intensity factors analysis of a v-notched three point bending specimen*

The stress intensity factor analysis of a v-notched three point bending specimen illustrated in Fig. 4 was performed using both the stress extrapolation method and the displacement extrapolation method. In this case, the orders of stress singularity, $1-\lambda_1$ and $1-\lambda_2$, are 0.456 and 0.091 respectively. Furthermore the mode II stress intensity factor $K_{II,\lambda_2}$ in Eq. 6 is always equal to zero because of the symmetric load condition. Therefore, Eq. 6 can be simplified as

$$\sigma_{kl,i} = \frac{K_{I,\lambda_1}}{r^{0.456}} f_{kl,i}^I(\theta) \tag{13}$$

The linear elastic finite element analysis of a v-notched three points bending specimen was performed using four types of the finite element mesh. The detail of each mesh around a corner is illustrated in Fig. 5; both of the minimum size of finite elements around the corner and the number of nodes of each mesh are shown in Tab. 1. The stress ahead of the corner and the displacement on the both surfaces of the v-notch were used for the stress and displacement extrapolation methods respectively. The obtained value of the stress intensity factor $K_{I,\lambda_1}$ is also shown in Tab. 1 for each mesh with the stress extrapolation method and the displacement extrapolation method. These results of the stress intensity factor analyses are non-

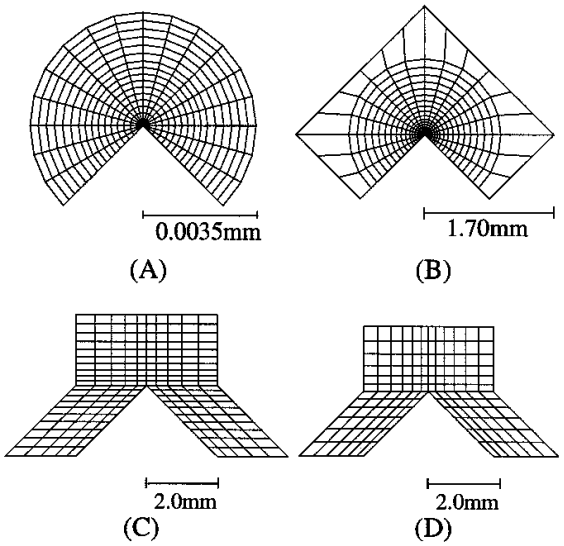


**Figure 5** : FEM meshes around the corner of a v-notch.

dimensionalized as

$$F_{I,\lambda_1} = \frac{K_{I,\lambda_1}}{\sigma_o \cdot a^{0.456}}, \quad \sigma_o = \frac{3SP}{2W^2} \tag{14}$$

where $a$ is a crack length, $\sigma_o$ a nominal stress, $S$ a span between fulcrums, $W$ a width of specimen, $P$ a load for a unit thickness of a plate. The stress extrapolation method cannot provide valid results by the mesh C and the mesh D because of the scattered nature of the numerical stress data. On the other hand, the displacement extrapolation method can give stable results for all the meshes. The difference between the $F_{I,\lambda_1}$ obtained by the mesh D and that by the mesh A is within 3%. Obviously, the displacement extrapolation method gives more reliable results than the stress extrapolation method.

To confirm the validity of the stress field in the close vicinity of the corner expected by the asymptotic equation together with the $K_{I,\lambda_1}$ obtained by the displacement extrapolation method, the stress field obtained from the Eq. 13 at $F_{I,\lambda_1} = 3.06$, the stress intensity factor obtained by the coarsest mesh D, is compared with that obtained directly by the finest mesh A at $P = 1.0 \times 10^4\, N/m$. Fig. 6 provides the angular variation of the hoop stress at 5.0 $\mu m$ from the corner, and Fig. 7 plots the hoop stress along the $x$-axis ahead of the corner. As shown in these Figures, the stress near the corner expected by the asymptotic equation together with the stress intensity factor obtained by the coarsest mesh is in good agreement with the stress field calculated using the finest mesh. The stress intensity factor of a corner can describe the stress field near the corner; it is expected to be useful for the strength evaluation of a corner in an electronic device.

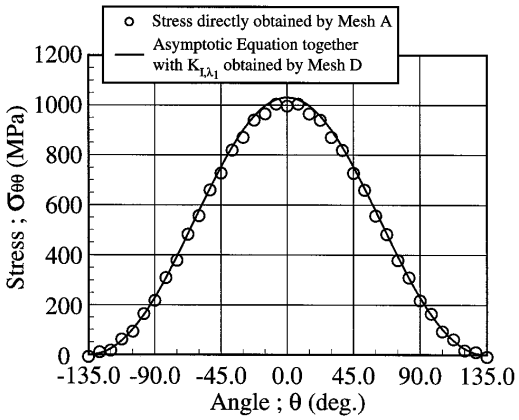


**Figure 6** : Angular variation of hoop stress at 5.0 $\mu m$ distant from the corner of a v-notch.

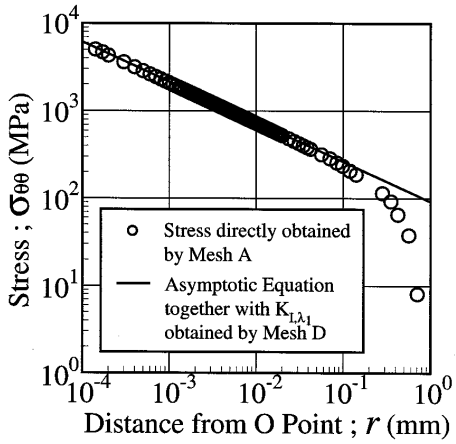


**Figure 7** : Stress distribution along the $x$-axis ahead of the corner of a v-notch.

## 4 Measurement of the fracture toughness of a corner in molding resin

We measured the fracture toughness of a v-notch in the molding resin A, which is the actual molding resin for common plastic packages. We measured it at three different temperatures, 20 $^oC$, 100 $^oC$ and 240 $^oC$, using v-notched three point bending specimens. The shape of the v-notched specimens is the same as that used for the numerical analysis as shown in Fig. 4, and the material properties of the molding resin A at respective temperatures are indicated in Tab. 2.

We carried out seven fracture tests for each temperature to obtain the fracture loads. The fracture loads measured by these tests are illustrated in Fig. 8. The data were scattered within a narrow band. The fracture toughness of a v-notch is calculated from the average of the fracture loads at each temperature by Eq. 14 and $F_{I,\lambda_1} = 2.99$, which obtained by the numerical

**Table 2** : Material properties and measured critical stress intensity factor of a v-notch for the molding resin a at each temperature.

| $T\ (^oC)$ | 20 | 100 | 240 |
|---|---|---|---|
| $E\ (GPa)$ | 18.6 | 15.8 | 1.07 |
| $\nu$ | 0.4 | 0.4 | 0.4 |
| CTE $(\times 10^6/K)$ | 13 | 13 | 49 |
| $K_{I\lambda_1 C}\ (Mpa \cdot m^{0.456})$ | 4.45 | 3.91 | 0.54 |

CTE: Coefficients of thermal expansion

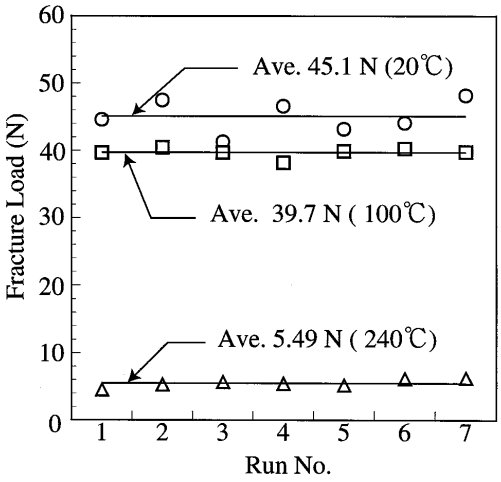


**Figure 8** : Fracture loads measured by the v-notched three points bending tests.

analysis with the finest mesh. The fracture toughness obtained at each temperature is indicated in Tab. 2 and illustrated in Fig. 9. Because the fracture toughness of the epoxy resin is well known to decrease dramatically around the glass transition temperature ($150\,^oC$), we guess that the fracture toughness changes like a broken line in Fig. 9.

## 5 Conclusion

We proposed the stress and the displacement extrapolation methods for calculating the stress intensity factors of a corner of joined dissimilar materials. The conclusions derived from the present paper are as follows.

1. The displacement extrapolation method can provide the accurate stress intensity factor of a corner of jointed dissimilar materials without a very fine finite element mesh.

2. The stress intensity factors obtained by the present method can well describe the stress field near the corner of a v-notch; it is expected to be useful for the strength evaluation of corners in electronic devices.

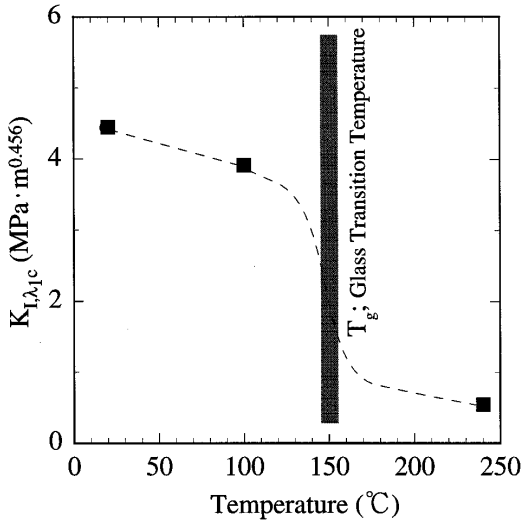


**Figure 9** : The critical stress intensity factor of a v-notch with the temperature.

3. The fracture toghness values of a v-notch at different temperatures are obtained by the v-notched three point bending tests and the present numerical method.

**Acknowledgement:** This study was performed as a project cooperated with FUJITSU LIMITED in the consortiums, RC-144 and RC-162, managed by the JSME. All specimens used in this research and some technical advices are provided by Mr. N. Ito, Ms. M. Nagatake, Mr. M. Sato and other related people in FUJITSU LIMITED. The support and encouragement are gratefully acknowledged.

## References

**Chen, D.; Nishitani, H.** (1991): Stress fields near the corner of jointed dissimilar materials. *Trans. JSME, Series A*, vol. 57, pp. 366–372.

**Dunn, M. L.; Suwito, W.** (1997): Fracture initiation at sharp notches: Correlation using critical stress intensities. *Int. J. Solids Structures*, vol. 34, pp. 3873–3883.

**Dunn, M. L.; Suwito, W.; Cunningham, S.; May, C. W.** (1997): Fracture initiation at sharp notches under mode I, mode II, and mild mixed mode loading. *Int. J. Fracture*, vol. 84, pp. 367–381.

**Hattori, T.; Nishimura, A.; Murakami, G.** (1990): A stress singularity parameter approach for evaluating reliability of LSI plastic package. *J. Society Material Science*, vol. 39, pp. 1101–1105.

**Ikeda, T.; Komohara, Y.; Miyazaki, N.** (1997): Measurement of mixed mode fracture toughness of an interface crack in electronic devises. *Advances in Electronic Packaging, ASME EEP.*, vol. 19, no. 2, pp. 1137–1444.

**Kitano, M.; Kawai, S.; Nishimura, A.; Nishi, K.** (1989): A study of package cracking during the reflow soldering process. *Trans. JSME, Series A*, vol. 55, pp. 356–363.

**Nishimura, A.; Hirose, I.; Tanaka, N.** (1993): A new method for measuring adhesion strength of IC molding compounds. *Trans. JSME Series A*, vol. 59, pp. 620–626.

**Nishimura, A.; Kawai, S.; Murakami, G.** (1989): Effect of lead frame material on plastic-encapsulated IC package cracking under temperature cycling. *IEEE Trans. Comp., Hybrids, Manufact. Tech.*, vol. 12, pp. 639–645.

**Nishimura, A.; Tatemichi, A.; Miura, H.; Sakamoto, T.** (1987): Life estimation for IC plastic packages under temperature cycling based on fracture mechanics. *IEEE Trans. Comp., Hybrids, Manufact. Tech.*, vol. CHMT-12, no. 4, pp. 637–642.

**Tanaka, N.; Nishiura, A.** (1994): Measurement of IC molding compound adhesion strength and prediction of interface delamination within package. *Trans. JSME Series A*, vol. 60, pp. 1992–1999.

**Williams, M. L.** (1952): Stress singularities resulting from various boundary conditions in angular corners of plates in extension. *J. Applied Mechanics*, vol. 74, pp. 526–528.

**Appendix A:**

The coefficient terms of the asymptotic solution as shown as Eq. 6 $f^I_{xx,i}(\theta)$, $f^{II}_{xx,i}(\theta)$, $f^I_{yy,i}(\theta)$, $f^{II}_{yy,i}(\theta)$, $f^I_{xy,i}(\theta)$, $f^{II}_{xy,i}(\theta)$ were presented by Chen and Nishitani (1991) as follows.

For material 1,

$$f^I_{xx,1}(\theta)=\frac{\lambda_1}{\sqrt{2\pi}(\alpha-\beta)}[[2(\alpha-\beta)\sin\{\lambda_1(\gamma-\pi)\}+\lambda_1(\alpha-\beta)\sin\{\gamma-\lambda_1(\gamma-\pi)\}-(1-\beta)\sin(\lambda_1\pi)]\times\cos\{(\lambda_1-1)\theta\}-[(\lambda_1-1)(\alpha-\beta)\sin\{\lambda_1(\gamma-\pi)\}]\times\cos\{(\lambda_1-3)\theta\}] \quad (15)$$

$$f^{II}_{xx,1}(\theta)=\frac{\lambda_2}{\sqrt{2\pi}(\alpha-\beta)}[[2(\alpha-\beta)\sin\{\lambda_2(\gamma-\pi)\}-\lambda_2(\alpha-\beta)\sin\{\gamma-\lambda_2(\gamma-\pi)\}+(1-\beta)\sin(\lambda_2\pi)]\times\sin\{(\lambda_2-1)\theta\}-[(\lambda_2-1)(\alpha-\beta)\sin\{\lambda_2(\gamma-\pi)\}]\times\sin\{(\lambda_2-3)\theta\}] \quad (16)$$

$$f^I_{yy,1}(\theta)=\frac{\lambda_1}{\sqrt{2\pi}(\alpha-\beta)}[[2(\alpha-\beta)\sin\{\lambda_1(\gamma-\pi)\}+\lambda_1(\alpha-\beta)\sin\{\gamma-\lambda_1(\gamma-\pi)\}+(1-\beta)\sin(\lambda_1\pi)]\times\cos\{(\lambda_1-1)\theta\}+[(\lambda_1-1)(\alpha-\beta)\sin\{\lambda_1(\gamma-\pi)\}]\times\cos\{(\lambda_1-3)\theta\}] \quad (17)$$

$$f^{II}_{yy,1}(\theta)=\frac{\lambda_2}{\sqrt{2\pi}(\alpha-\beta)}[[2(\alpha-\beta)\sin\{\lambda_2(\gamma-\pi)\}+\lambda_2(\alpha-\beta)\sin\{\gamma-\lambda_2(\gamma-\pi)\}-(1-\beta)\sin(\lambda_2\pi)]\times\sin\{(\lambda_2-1)\theta\}+[(\lambda_2-1)(\alpha-\beta)\sin\{\lambda_2(\gamma-\pi)\}]\times\sin\{(\lambda_2-3)\theta\}] \quad (18)$$

$$f^I_{xy,1}(\theta)=\frac{\lambda_1}{\sqrt{2\pi}(\alpha-\beta)}[[\lambda_1(\alpha-\beta)\sin\{\gamma-\lambda_1(\gamma-\pi)\}+(1-\beta)\sin(\lambda_1\pi)]\times\sin\{(\lambda_1-1)\theta\}+[(\lambda_1-1)(\alpha-\beta)\sin\{\lambda_1(\gamma-\pi)\}]\times\sin\{(\lambda_1-3)\theta\}] \quad (19)$$

$$f^{II}_{xy,1}(\theta)=\frac{\lambda_2}{\sqrt{2\pi}(\alpha-\beta)}[[-\lambda_2(\alpha-\beta)\sin\{\gamma-\lambda_2(\gamma-\pi)\}+(1-\beta)\sin(\lambda_2\pi)]\times\cos\{(\lambda_2-1)\theta\}-[(\lambda_2-1)(\alpha-\beta)\sin\{\lambda_2(\gamma-\pi)\}]\times\cos\{(\lambda_2-3)\theta\}] \quad (20)$$

For material 2,

$$f^I_{xx,2}(\theta)=\frac{C_1\lambda_1}{\sqrt{2\pi}(\alpha-\beta)}[[-2(\alpha-\beta)\sin\{\lambda_1(\gamma-\pi)\}+\lambda_1(\alpha-\beta)\sin\{\gamma-\lambda_1(\gamma-\pi)\}+(1+\beta)\sin(\lambda_1\pi)]\times\cos\{(\lambda_1-1)(\pi-\theta)\}+[(\lambda_1-1)(\alpha-\beta)\sin\{\lambda_1(\gamma-\pi)\}]\times\cos\{(\lambda_1-3)(\pi-\theta)\}] \quad (21)$$

$$f^{II}_{xx,2}(\theta)=\frac{C_2\lambda_2}{\sqrt{2\pi}(\alpha-\beta)}[[2(\alpha-\beta)\sin\{\lambda_2(\gamma-\pi)\}-\lambda_2(\alpha-\beta)\sin\{\gamma-\lambda_2(\gamma-\pi)\}+(1+\beta)\sin(\lambda_2\pi)]\times\sin\{(\lambda_2-1)(\pi-\theta)\}-[(\lambda_2-1)(\alpha-\beta)\sin\{\lambda_2(\gamma-\pi)\}]\times\sin\{(\lambda_2-3)(\pi-\theta)\}] \quad (22)$$

$$f^I_{yy,2}(\theta)=\frac{C_1\lambda_1}{\sqrt{2\pi}(\alpha-\beta)}[[-2(\alpha-\beta)\sin\{\lambda_1(\gamma-\pi)\}-\lambda_1(\alpha-\beta)\sin\{\gamma-\lambda_1(\gamma-\pi)\}-(1+\beta)\sin(\lambda_1\pi)]\times\cos\{(\lambda_1-1)(\pi-\theta)\}-[(\lambda_1-1)(\alpha-\beta)\sin\{\lambda_1(\gamma-\pi)\}]\times\cos\{(\lambda_1-3)(\pi-\theta)\}] \quad (23)$$

$$f^{II}_{yy,2}(\theta)=\frac{C_2\lambda_2}{\sqrt{2\pi}(\alpha-\beta)}[[2(\alpha-\beta)\sin\{\lambda_2(\gamma-\pi)\}+\lambda_2(\alpha-\beta)\sin\{\gamma-\lambda_2(\gamma-\pi)\}-(1+\beta)\sin(\lambda_2\pi)]\times\sin\{(\lambda_2-1)(\pi-\theta)\}+[(\lambda_2-1)(\alpha-\beta)\sin\{\lambda_2(\gamma-\pi)\}]\times\sin\{(\lambda_2-3)(\pi-\theta)\}] \quad (24)$$

$$f^{I}_{xy,2}(\theta) = \frac{C_1\lambda_1}{\sqrt{2\pi}(\alpha-\beta)}\,[[\lambda_1(\alpha-\beta)\sin\{\gamma-\lambda_1(\gamma-\pi)\} + (1+\beta)\sin(\lambda_1\pi)]\times\sin\{(\lambda_1-1)(\pi-\theta)\} + [(\lambda_1-1)(\alpha-\beta)\sin\{\lambda_1(\gamma-\pi)\}] \times\sin\{(\lambda_1-3)(\pi-\theta)\}] \tag{25}$$

$$f^{II}_{xy,2}(\theta) = \frac{C_2\lambda_2}{\sqrt{2\pi}(\alpha-\beta)}\,[[\lambda_2(\alpha-\beta)\sin\{\gamma-\lambda_2(\gamma-\pi)\} - (1+\beta)\sin(\lambda_2\pi)]\times\cos\{(\lambda_2-1)(\pi-\theta)\} + [(\lambda_2-1)(\alpha-\beta)\sin\{\lambda_2(\gamma-\pi)\}] \times\cos\{(\lambda_2-3)(\pi-\theta)\}] \tag{26}$$

$$C_1 = [(1-\beta)\sin(\lambda_1\gamma) + (1-\alpha)\sin\{\lambda_1(\pi-\gamma)\} + \lambda_1(\alpha-\beta)\sin\gamma]\,/\,[(1+\beta)\sin\{\lambda_1(2\pi-\gamma)\} + (1+\alpha)\sin\{\lambda_1(\gamma-\pi)\} + \lambda_1(\alpha-\beta)\sin\gamma] \tag{27}$$

$$C_2 = [(1-\beta)\sin(\lambda_2\gamma) + (1-\alpha)\sin\{\lambda_2(\pi-\gamma)\} - \lambda_2(\alpha-\beta)\sin\gamma]\,/\,[(1+\beta)\sin\{\lambda_2(2\pi-\gamma)\} + (1+\alpha)\sin\{\lambda_2(\gamma-\pi)\} - \lambda_2(\alpha-\beta)\sin\gamma] \tag{28}$$

**Appendix B:**

The explicit asymptotic solution of the displacement is derived from the stress function obtained by Chen and Nishitani (1991) as follows.

The displacement around a corner is expressed as the next equation using complex stress functions $\phi(z)$ and $\psi(z)$.

$$u_i + iv_i = \frac{1}{2G_i}\left\{\kappa_i\phi_i(z) - z\overline{\phi_i'}(z) - \overline{\psi_i}(z)\right\} \tag{29}$$

where the subscript $i$ takes material 1 ($i=1$) or material 2 ($i=2$), $i$ is the complex number ($i^2=-1$), $z$ is the coordinates of complex number, $z=x+iy$, and the upper bar denotes the conjugate. Chen and Nishitani (1991) derived the stress functions in Eq. 29 for the symmetric deformation to the $x$-axis (Mode I) as

$$\begin{cases} \phi_1(z) = (a_{11}+\overline{a_{11}})z^{\lambda_1} = (a_{11}+\overline{a_{11}})\,r^{\lambda_1}e^{i\lambda_1\theta} \\ \phi_1'(z) = (a_{11}+\overline{a_{11}})\lambda_1 z^{\lambda_1-1} = \\ \qquad (a_{11}+\overline{a_{11}})\,\lambda_1 r^{\lambda_1-1}e^{i(\lambda_1-1)\theta} \\ z\overline{\phi_1'(z)} = z'(a_{11}+\overline{a_{11}})\lambda_1 z^{\lambda_1-1}e^{i(1-\lambda_1)\theta} = \\ \qquad (a_{11}+\overline{a_{11}})\,\lambda_1 r^{\lambda_1}e^{i(2-\lambda_1)\theta} \\ \overline{\psi_1(z)} = (b_{11}+\overline{b_{11}})\overline{z^{\lambda_1}} = (b_{11}+\overline{b_{11}})r^{\lambda_1}e^{-i\lambda_1\theta} \end{cases} \tag{30}$$

where

$$a_{11}+\overline{a_{11}} = \frac{K_{I,\lambda_1}}{\sqrt{2\pi}}\sin(\lambda_1(\gamma-\pi)) = \frac{K_{I,\lambda_1}}{\sqrt{2\pi}}A_1^I \tag{31}$$

$$b_{11}+\overline{b_{11}} = \frac{K_{I,\lambda_1}}{\sqrt{2\pi}(\alpha-\beta)}\{\lambda_1(\alpha-\beta)\sin(\gamma-\lambda_1(\gamma-\pi)) + (1-\beta)\sin(\lambda_1\pi)\} = \frac{K_{I,\lambda_1}}{\sqrt{2\pi}}B_1^I \tag{32}$$

The explicit displacement field around a corner for Mode I deformation is obtained from the Eq. 29 and Eq. 30.

$$u_1 + iv_1 = \frac{r^{\lambda_1}K_{I,\lambda_1}}{2\sqrt{2\pi}G_1}\left\{\kappa_1 A_1^I e^{i\lambda_1\theta} - A_1^I\lambda_1 e^{i(2-\lambda_1)\theta} - B_1^I e^{-i\lambda_1\theta}\right\} \tag{33}$$

Therefore

$$u_1^I = \frac{r^{\lambda_1}K_{I,\lambda_1}}{2\sqrt{2\pi}G_1}\left\{(A_1^I\kappa_1 - B_1^I)\cos(\lambda_1\theta) - A_1^I\lambda_1\cos((2-\lambda_1)\theta)\right\}$$
$$v_1^I = \frac{r^{\lambda_1}K_{I,\lambda_1}}{2\sqrt{2\pi}G_1}\left\{(A_1^I\kappa_1 + B_1^I)\sin(\lambda_1\theta) + A_1^I\lambda_1\sin((2-\lambda_1)\theta)\right\} \tag{34}$$

In case of the skew-symmetric deformation to the $x$-axis (Mode II), Chen and Nishitani (1991) also obtained the stress functions as

$$\begin{cases} \phi_1(z) = (a_{11}-\overline{a_{11}})z^{\lambda_2} = (a_{11}-\overline{a_{11}})\,r^{\lambda_2}e^{i\lambda_2\theta} \\ z\overline{\phi_1'(z)} = -(a_{11}-\overline{a_{11}})\lambda_2 r^{\lambda_2}e^{i(2-\lambda_2)\theta} \\ \overline{\psi_1(z)} = (\overline{b_{11}}-b_{11})\overline{z^{\lambda_2}} = -(b_{11}-\overline{b_{11}})\,r^{\lambda_2}e^{-i\lambda_2\theta} \end{cases} \tag{35}$$

where

$$a_{11}-\overline{a_{11}} = -i\frac{K_{II,\lambda_2}}{\sqrt{2\pi}}\sin(\lambda_2(\gamma-\pi)) = -i\frac{K_{II,\lambda_2}}{\sqrt{2\pi}}A_1^{II} \tag{36}$$

$$b_{11}-\overline{b_{11}} = -i\frac{K_{II,\lambda_2}}{\sqrt{2\pi}(\alpha-\beta)}\{\lambda_2(\alpha-\beta)\sin(\gamma-\lambda_2(\gamma-\pi)) - (1-\beta)\sin(\lambda_2\pi)\} = -i\frac{K_{II,\lambda_2}}{\sqrt{2\pi}}B_1^{II} \tag{37}$$

The explicit displacement field around a corner for Mode II deformation is also obtained from Eq. 29 and Eq. 35.

$$u_1 + iv_1 = -i\frac{r^{\lambda_2}K_{II,\lambda_2}}{2\sqrt{2\pi}G_1}\left\{\kappa_1 A_1^{II}e^{i\lambda_2\theta} + A_1^{II}\lambda_2 e^{i(2-\lambda_2)\theta} + B_1^{II}e^{-i\lambda_2\theta}\right\} \tag{38}$$

Therefore,

$$u_1^{II} = \frac{r^{\lambda_2}K_{II,\lambda_2}}{2\sqrt{2\pi}G_1}\left\{(A_1^{II}\kappa_2 - B_1^{II})\sin(\lambda_2\theta) + A_1^{II}\lambda_2\sin((2-\lambda_2)\theta)\right\}$$
$$v_1^{II} = \frac{r^{\lambda_2}K_{II,\lambda_2}}{2\sqrt{2\pi}G_1}\left\{(A_1^{II}\kappa_2 + B_1^{II})\cos(\lambda_2\theta) + A_1^{II}\lambda_2\cos((2-\lambda_2)\theta)\right\} \tag{39}$$